Proceedings of IDETC/CIE 2020
The ASME 2020 International Design Engineering Technical Conferences &
Computers and Information in Engineering Conference
August 16 – 19, 2020, St. Louis, MO, USA

IDETC2020-22035

A CONTINUOUSLY TUNABLE STIFFNESS ARM WITH CABLE-DRIVEN MECHANISMS FOR SAFE PHYSICAL HUMAN-ROBOT INTERACTION

Yu She

Computer Science and
Artificial Intelligence Laboratory
Massachusetts Institute of Technology
Cambridge, MA 02139
Postdoctoral Associate
Email: yushe@mit.edu

Zhaoyuan Gu

Department of Mechanical Engineering
Carnegie Mellon University
Pittsburgh, PA 15213
Graduate student
Email:zhaoyuan@andrew.cmu.edu

Siyang Song

Walker Department of
Mechanical Engineering
University of Texas at Austin
Austin, Texas 78712
Graduate Research Associate
Email: sysong@utexas.edu

Hai-Jun Su

Department of Mechanical and
Aerospace Engineering
Ohio State University
Columbus, Ohio 43210
ASME Fellow, Professor
Email: su.298@osu.edu

Junmin Wang

Walker Department of
Mechanical Engineering
University of Texas at Austin
Austin, Texas 78712
ASME Fellow, Professor
Email:JWang@austin.utexas.edu

ABSTRACT

In this paper, we present a continuously tunable stiffness arm for safe physical human-robot interactions. Compliant joints and compliant links are two typical solutions to address safety issues for physical human-robot interaction via introducing mechanical compliance to robotic systems. While extensive studies explore variable stiffness joints/actuators, variable stiffness links for safe physical human-robot interactions are much less studied. This paper details the design and modeling of a compliant robotic arm whose stiffness can be continuously tuned via cable-driven mechanisms actuated by a single servo motor. Specifically, a 3D printed compliant robotic arm is prototyped and tested by static experiments, and an analytical model of the variable stiffness arm is derived and validated by testing. The results show that the lateral stiffness of the robot arm can achieve a variety of 221.26 % given a morphing angle of 90°. The study demonstrates that the compliant link design could be a promising approach to address safety concerns for safe physical human-robot interactions.

1 Introduction

As robots become increasingly integrated with humans in various domains [1], safety becomes a prominent consideration in physical human-robot interactions. To increase the safety for physical human-robot interaction, researchers have introduced mechanical compliance to robots, either in robot's joints

or links. Extensive research has been conducted on joint compliance, while limited studies have explored link compliance.

A typical example of joint compliance is the anthropomorphic hand system [2, 3, 4], where superimposed cam mechanisms and floating springs are employed at the joint such that kinetic energy from an impact could be absorbed and stored to the springs. Other classic joint compliance designs include the variable impedance actuation (VIA) and variable stiffness actuators (VSA) [5, 6, 7, 8]. Their joint stiffness is able to change rapidly and continuously to satisfy the safety requirements. More research on the VSA includes [9, 10, 11, 12].

Compared with the joint compliance, the link compliance is much less explored [13, 14]. Researchers developed switch compliant links to ensure safety [15, 16, 17]. The basic idea is that the robot link is rigid for normal operation but could switch to a compliant mode given an external force exceeding a threshold. An inherently safe robotic arm is developed in [18, 19] via optimization of the beam profile. Unlike the VSA, in which joint stiffness is continuously adjustable, all of these switch designs do not offer continuously controllable stiffness. Although tunable stiffness links are developed in a variety of applications such as flapping-wing robots [20] and legged robots [21], few of them are employed in physical human-robot interactions [22, 23].

Modeling compliant links is more complex than modeling compliant joints since it contains an infinite degree of freedoms. However, the pseudo-rigid-body (PRB) model [24,25] provides a simple and efficient solution for modeling compliant links especially in the initial design stage, which will be used and discussed in this paper.

In this paper, we propose a new compliant robotic arm for physical human-robot interaction. The stiffness of the arm can be continuously tuned by morphing the shape of the arm, i.e. changing the second moment of inertia of the cross section via a set of cable-driven mechanisms.

We start this paper with the motivation for this research in Sec.2. The mechanical design of the morphing arm and the associated cable-driven mechanism is presented in Sec.3. In Sec.4, kinetostatic (kinematic and static) analysis of the cable-driven mechanisms and the variable stiffness modeling of the shape morphing arm are derived. A 3D printed prototype and extensive experiments are presented in Sec.5, followed by discussion in Sec.6. Finally, conclusions are addressed in Sec.7.

2 Motivations

In a typical rest-to-rest task, a robot generally performs as follows: 1) it increases its speed from 0 during the first stage, 2) it reaches a stable maximum speed in the second stage to increase the time efficiency, 3) it gradually reduces its speed to 0 and finally reaches the destination at the end of the third stage. A schematic view of the velocity variation $v(t)$ is shown in Fig. 1.

A high operation speed of the manipulator may be desired from the perspective of time efficiency, while high safety is required for physical human-robot interaction. When an unexpected collision occurs between a human and a traditional robot with constant stiffness, fast motion permits high efficiency but may cause a severe injury, while slow motion may admit high safety but corresponds to low efficiency. If we can actively tune down the robot's stiffness during the high speeds and tune up the stiffness during the low speed, high performance and high safety may be obtained simultaneously. A schematic view of the corre-

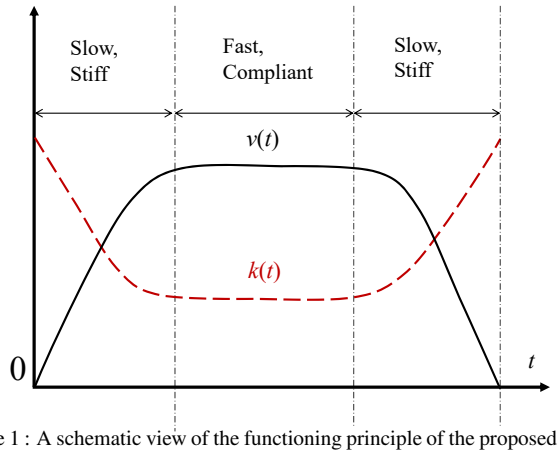

Figure 1 : A schematic view of the functioning principle of the proposed morphing arm concept for a typical rest-to-rest task. The arm is in the stiff mode given slow motion while it is switched in compliant mode given fast motion.

Therefore, there is a need to develop robotic arms with tunable stiffness to address the aforementioned paradox. A robot arm with tunable stiffness may potentially address the two competing criteria: high performance and high safety, which will be the focus of this study. There are a few methods to achieve the stiffness variation of the robot arm such as tuning the second moment of inertia, controlling effective length, changing material modulus, etc. In this study, we adopt the shape morphing solution, i.e., changing the second moment of inertia to obtain the tunable stiffness via cable-driven mechanisms.

3 The mechanical design

In this section, we detail the mechanical design of the shape morphing arm and the associated cable-driven mechanisms.

3.1 Mechanical design of the shape morphing arm

The shape morphing arm is comprised of a servo motor, four pairs of bearing frame, two universal transmission shaft, a base house, an end house, an end load, two flexible beams, and three

cable-driven mechanisms as shown in Fig. 2. The key components are the flexible beams that are assembled on both sides of the morphing arm, which are the source of the variable lateral stiffness. The flexible beams are flattened in Fig. 2 under a compliant mode, and they can be morphed in curved shapes under stiff modes via cable-driven mechanisms. The variable stiffness

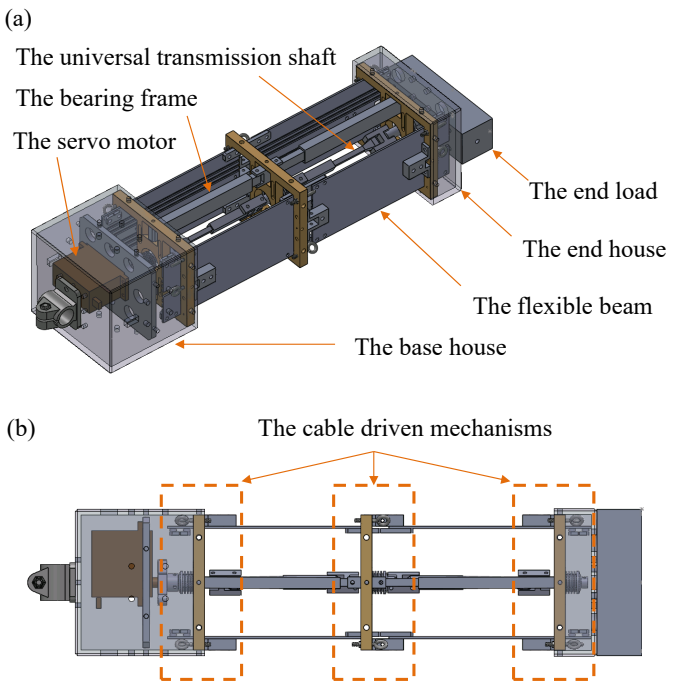

Figure 2 : The design of the proposed shape morphing arm.

In addition to the variable lateral stiffness, we would lik maintain the high rigidity in the vertical direction for the purp of carrying loads. Therefore, four bearing frames are desig to connect the cable-driven mechanisms. The left cable-dri mechanism is fixed on the base house and the right cable-dri mechanism is attached to the end house. The bearing frai are designed as a square rail with linear guides permitting ext sion and contraction, and the connections between the bear frames and cable-driven mechanisms are rotational joints in lateral direction. As a result, the shape morphing arm behave a compliant parallel-guiding mechanism while it remains rigi the vertical direction given lateral forces.

A servo motor sitting in the base house provides torque to morph the flexible beams via cable-driven mechanisms. In order to morph the flexible beam uniformly, three cable-driven mechanisms are assembled and distributed along the morphing arm. To reduce the number of the actuators, two universal transmission shafts are designed to connect the three cable-driven mechanisms such that a single servo motor can actuate all cable-driven mechanisms simultaneously, and further morph the flexible beam uniformly.

The central line of the flexible beams are assembled on the cable-driven mechanisms, while the up edge and bottom edge of the flexible beams are connected with cables for the morphing purpose. The base house, the end house, the cable-driven mechanisms and the bearing frames basically form the "skeletons", while the flexible beams comprise the "muscles" of the shape morphing arm.

3.2 Detailed design of the cable-driven mechanism

The detailed design of the cable-driven mechanism is presented in this section. The three cable-driven mechanisms are identical and the detailed design is shown in Fig. 3. The bold dashed lines represent the flattened shape of the flexible beams under the compliant mode, while the bold solid lines represent the curved shape of the beams under stiff mode. There are four cable loops in each cable-driven mechanism, including L_1, L_2, L_3, and L_4, from which the diagonal loops share the same winding route and the adjacent loops have slightly different windings around the center pulley. Each cable loop goes through four pulleys including the center pulley, bending control pulley, recovering control pulley and the base pulley. The pulleys are placed

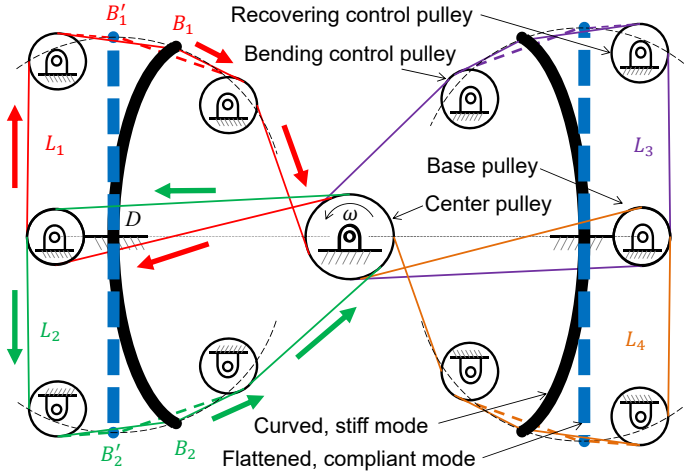

Figure 3 : The design of the cable-driven mechanism.

We take the loops of L_1 and L_2 as examples to illustrate how the cable-driven mechanism achieves the shape morphing via the servo motor. Starting from L_1 under the flattened shape, the cable is attached at and starts from the edge of the flexible beam B_1'. After winding through a few pulleys the cable ends with and

is attached at B_1' in a loop. By following the arrow directions, the route of L_1 (L_3) can be described as $B_1' \rightarrow$ bending control pulley $\rightarrow$ center pulley $\rightarrow$ base pulley $\rightarrow$ recovering control pulley $\rightarrow B_1'$. Similarity, the route of L_2 (L_3) can be described as $B_2' \rightarrow$ bending control pulley $\rightarrow$ center pulley $\rightarrow$ base pulley $\rightarrow$ recovering control pulley $\rightarrow B_2'$. Given a counter-clockwise motor torque, the flexible beams are pulled from the flattened shape (B_1' and B_2') to the curved shape (B_1 and B_2), and vice versa. The four cable loops allow the shape morphing of the flexible beam symmetrically and the three cable-driven mechanisms permit the shape morphing uniformly.

For the purpose of simplicity, the bending control pulley and recovering control pulley are not necessary. However, we intentionally designed these pulleys in order to enhance the moment arm of the flexible beam to reduce the motor torque for bending or recovering of the flexible beams. These pulleys are placed at positions in order to have the cable perpendicular to (approximately) the flexible beams.

4 Modeling of the morphing arm

In this sections, we study the kinematics of the cable-driven mechanism, the static models of the flexible beams, as well as the lateral stiffness models of the shape morphing arm.

4.1 Kinematics of the cable-driven mechanism

Considering the cross-section plane of the flexible beam, it is observed that the flexible beam is actually an initially straight pinned-pinned beam, which is fixed in the middle (Point D in Fig. 3) via attaching on the cable-driven mechanisms and is deformed at the edges (Point B_1' and B_2' in Fig. 3) by pulling the cables.

The PRB model is used here to model the kinematics of the flexible beams. Due to similarity, we only need to analyze one cable loop, e.g. the upper right loop L_3 as shown in Fig. 4 (a), and its PRB model is shown in Fig. 4 (b). Assume the flexible beam has a height, thickness, and length of l, t, and L respectively. Assume the two flexible beams are spaced with a distance of w. If we use r_4 to represent the length of the PRB link, it can be calculated by

$$r_4 = \frac{\gamma l}{2}, \tag{1}$$

where γ is the character radius factors. The stiffness of the torsional spring of the PRB model can be calculated as

$$k_c = \frac{\gamma K_\theta E I_z}{l/2}, \tag{2}$$

where K_θ is the stiffness constant of the PRB model and $I_z =$

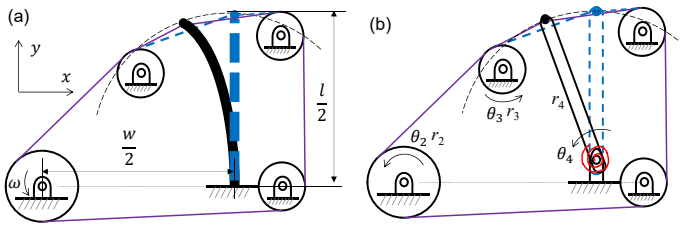

Figure 4 : (a) The cable loop with the flexible beam, (b) The cable loop with the PRB model.

Assume r_2 and r_3 represent the radius of the center pulley and the bending control pulley, and θ_2, θ_3, and θ_4 are rotation angles of the center pulley, the bending control pulley, and the PRB link, respectively. The motion of the pulleys satisfies the relation $\theta_2 r_2 = \theta_3 r3 \approx \theta_4 r_4$. Given the input angle θ_2 from the servo motor, the angle θ_4 can be calculated by

$$\theta_4 \approx \frac{r_2 \theta_2}{r_4} \tag{3}$$

We next specify actuation torque of the servo motor with further kinematics analysis. The parameters are labeled as shown in Fig. 5. Let A_0 and O_0 represent the rotation center of the center pulley and the bending control pulley. B_0 is the rotation center of the PRB link r_4. The coordinates of A_0, O_0, and B_0 are (0, 0), (c, d), and ($w/2$, $l/2$ - r_4) respectively. The distance δ between O_0 and B_0 can be calculated as

$$\delta = \sqrt{(\frac{w}{2} - c)^2 + (d - \frac{(1-\gamma)l}{2})^2} \tag{4}$$

Assume B' represents the end position of the link r_2 under the flattened shape, and B represents its arbitrary morphed location. B' has a constant coordinate of ($w/2$, $l/2$). The angle ϕ between O_0B_0 and $B'B_0$ is also a constant and can be calculated by

$$\phi = \arccos\left(\frac{d - \frac{(1-\gamma)l}{2}}{\delta}\right) \tag{5}$$

The angle η between O_0B_0 and BB_0 can be expressed as

$$\eta = \phi - \theta_4 \tag{6}$$

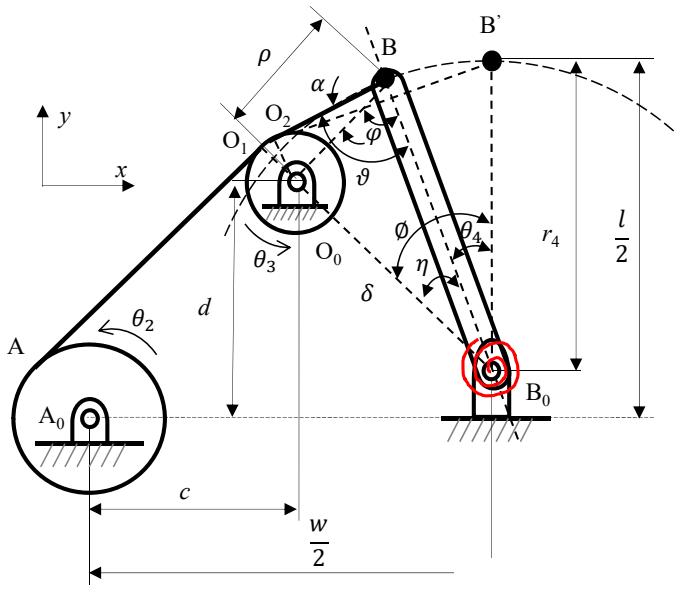

Figure 5 : The parameters of the cable loop w

The distance ρ between point B and O_0

$$\rho = \sqrt{\delta^2 + r_4^2 - 2\delta r_4 \cos}$$

The angle φ between BO_0 and BB_0 can

$$\varphi = \arccos\left(\frac{\rho^2 + r_4^2 - \delta^2}{2\rho r_4}\right)$$

Assume O_1 and O_2 are the points of tl the cable and the bending control pulley, BO_2 and BO_0 is

$$\alpha = \arcsin\left(\frac{r_3}{\rho}\right)$$

Then we can calculate the force direct between BO_2 and the PRB link

$$\vartheta = \alpha + \varphi$$

Consider a single cable loop, the intern ble can be calculated as follows to overcon torsional springs

$$F_c = \frac{k_c \theta_4}{r_4 \sin\vartheta} \tag{11}$$

Finally, consider four similar cases with a single servo motor, the required torque can be stated as

$$\tau = 4F_c r_2 \tag{12}$$

Table 1 : Geometric parameters of the cable-driven mechanism and the morphing arm

Parameters	Value (mm)	Parameters	Value (mm)
L	400	l	70
t	2	w	95
c	16	d	30
r_2	8	r_3	1

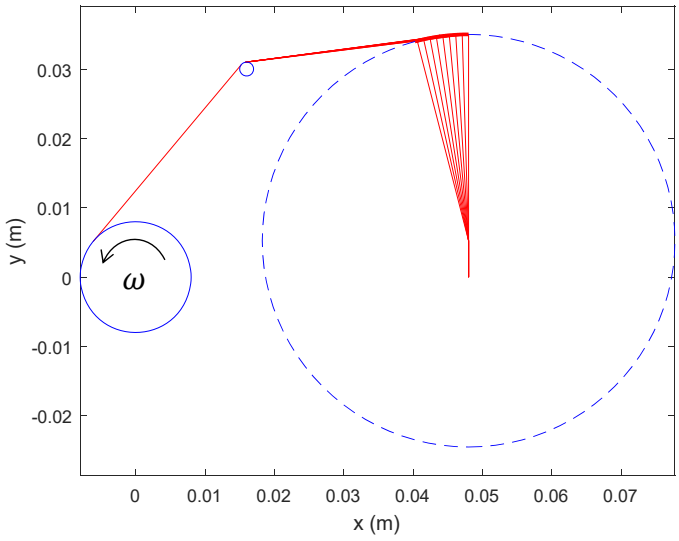

Figure 6 : The kinematics simulation of the cable-driven mechanism.

4.2 Mechanics of the flexible beams

The PRB model provides a convenient way for kinematics analysis and torque identification. However, it can not provide the exact shape of the flexible beams which is required for calculating the variable stiffness. Therefore, we will derive the static

model for the flexible beams under large deformations. Recall the flexible beam has a length, height, and thickness of L, l, and t, respectively. Assume the material of the beam is with Young's modulus of E. Given an actuation from the center pulley, the flexible beam may deform as shown in Fig. 7 (a). The flexible beam is actually a pinned-pinned segment. If we consider half of the segment, it can be modeled with a cantilever beam as shown

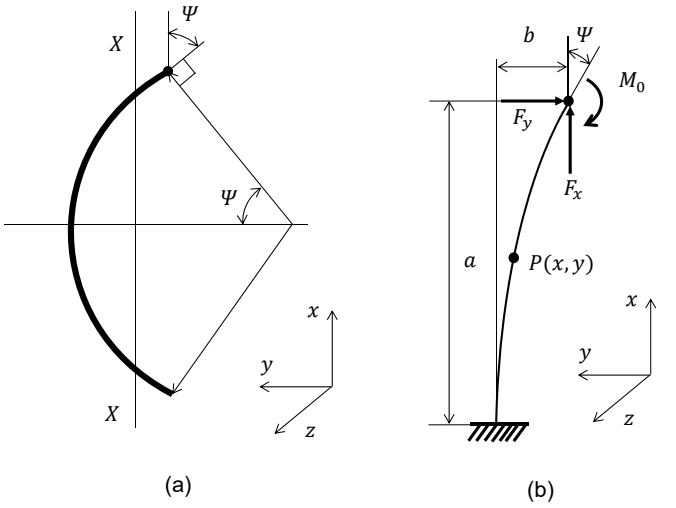

Figure 7 : (a) The deformed shape of the flexible beam, (b) The cantilever model of the flexible beam

Given external forces of F_x and F_y and an external moment of M_0 at the tip of the cantilever beam, it has a tip deformation of (a,b) and tip deformation angle of Ψ. The moment along the beam in an arbitrary point $P(x,y)$ can be expressed as

$$M(x,y) = F_x(y-b) + F_y(a-x) + M_0 \tag{13}$$

The Bernoulli-Euler equation is

$$\frac{d\theta}{ds} = \frac{M(x,y)}{EI_z}, \tag{14}$$

where I_z is the second moment of inertia in the z-axis direction and can be calculated by $I_z = Lt^3/12$. Eq. (14) takes derivative to s we have

$$\frac{d^2\theta}{ds^2} = \frac{1}{EI_z}(F_x \sin\theta(s) - F_y \cos\theta(s)) \tag{15}$$

Given the initial condition of $\theta(0) = 0$ and $\theta'(L) = M_0/EI_z$, we can calculate the lateral displacement of b and lateral deformation angle of Ψ. It is worth noting that Ψ is the tip deformation angle of half of the flexible beam, and the morphing angle of the entire flexible beam should be calculated as

$$\Omega = 2\Psi \tag{16}$$

Remember in this study the purpose of the shape morphing is to change the second moment of inertia of I_{XX}, where $_{XX}$ is the centroid axis of the deformed flexible beam as shown in Fig. 7 (a). The location of the centroid axis can be expressed as

$$\bar{y} = \frac{\int_A y dA}{A}, \tag{17}$$

where A is the cross section of the flexible beam of $A = lt$. Then the second moment of inertia of the deformed flexible beam can be calculated by

$$I_{XX} = \int_A \bar{y}^2 dA \tag{18}$$

In this study, only external forces (no external moments) are applied at the tip of the flexible beams. We can find the morphing angle Ω from Eq. (15) and the second moment of inertia I_{XX} from Eq. (18) for the flexible beam. Here we consider a simple situation that the mapping from Ω to I_{XX} is bijective and an Ω corresponds to a unique $I_{XX}(\Omega)$.

4.3 Lateral stiffness of the morphing arm with the classical PRB model

The shape morphing arm is actually a compliant parallelogram mechanism shown in Fig.8 (a), and it can be modeled by a classical fixed-guided PRB model as shown in Fig.8 (b). Considering a lateral force F applied at the stage, the PRB model has a lateral displacement x and a deflection angle β. The link lengths of the PRB model are l_1, l_2, and l_3 and can be calculated by

$$\begin{cases} l_1 = l_3 = (1-\gamma)L/2 \\ l_2 = \gamma L \end{cases} \tag{19}$$

The four torsional springs of the fixed-guided PRB model are identical and the stiffness of each spring can be calculated by

$$k_{fg}(\Omega) = \frac{2\gamma K_\theta E I_{xx}(\Omega)}{L} \tag{20}$$

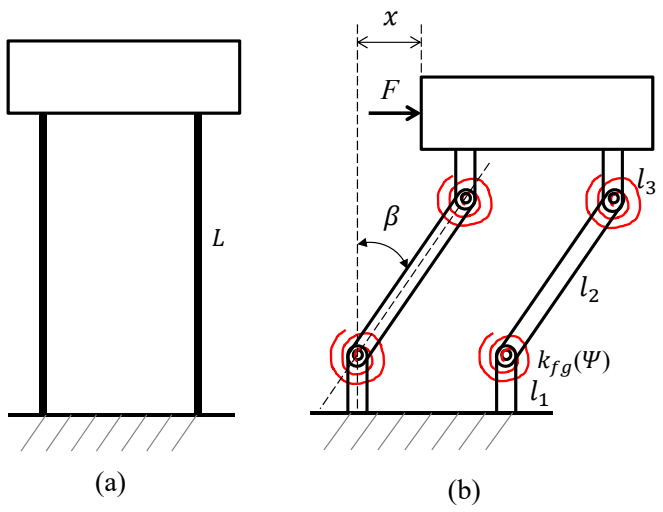

Figure 8 : (a) The compliant parallelogram mechanism, (b) The fixed-guided PRB model for lateral stiffness.

It is worth noting that in this paper the continuc variation is realized by morphing the shape of the fl with an angle Ω, i.e. tuning the second moment of in

The potential energy of the four torsional spring culated by

$$V = 2k_{fg}(\Omega)\beta^2$$

By virtual work principle, we have

$$F\delta x - \frac{dV}{d\beta}\delta\beta = 0$$

Then we can calculate the lateral force in term flection angle

$$F = \frac{4k_{fg}(\Omega)\beta}{\gamma L\cos\beta}$$

We further can calculate the lateral stiffness of th arm

$$K_\delta(\Omega,\beta) = \frac{dF}{dx} = \frac{4}{\gamma^2 L^2}k_{fg}(\Omega)\frac{(\cos\beta+\beta\sin\beta)}{\cos^3\beta} \qquad (24)$$

However, the original PRB model is not sufficiently accurate when compared with our later experimental results. The major problem is that the original PRB model assumes an ideal boundary condition, i.e. the flexible beams are rigidly fixed on both end houses. As a matter of fact, this assumption is not valid in this case. The middle part of the flexible beams (Point D in Fig. 3) is rigidly fixed on the cable-driven mechanisms while the bottom/up edges (Point B_1' and B_2' in Fig. 3) are not fixed since they need to be morphed. In fact, the rigidity at B_1' and B_2' depends on the stall torque of the servo motor and the cable extensibility. That is to say, the boundary condition of the flexible beams is significantly affected by those factors. In order to improve the accuracy of the lateral stiffness model, we consider the compliance of the connection parts between the flexible beams and houses, and we model the compliance using four identical torsional springs.

4.4 An improved PRB model for the lateral stiffness of the morphing arm

In addition to the four torsional springs of the original PRB model, we model the compliance from the boundary condition with four identical torsional springs k_b, and the improved lateral stiffness model is shown in Fig. 9. Considering a lateral force of

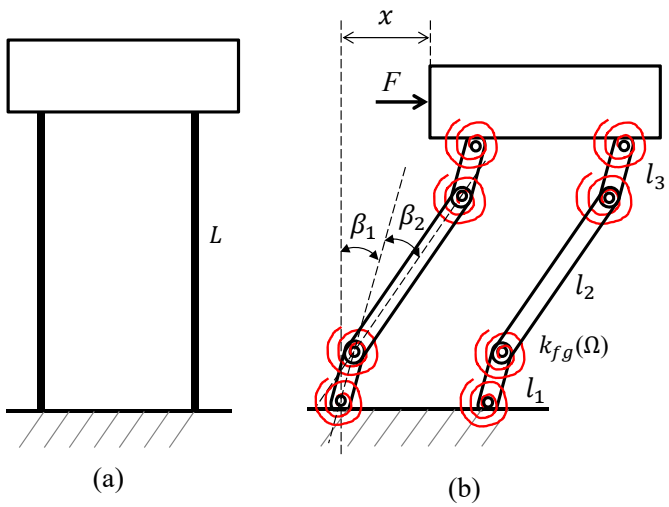

Figure 9 : (a) The compliant parallelogram mechanism, (b) The improved PRB model.

The lateral displacement can be calculated by

$$x = (1-\gamma)L\sin\beta_1 + \gamma L\sin(\beta_1+\beta_2) \qquad (25)$$

The lateral force in terms of the deformation angles can be calculated as follows

$$F = 4k_b\beta_1\frac{1}{(1-\gamma)L\cos\beta_1 + \gamma L\cos(\beta_1+\beta_2)} \qquad (26)$$

$$F = \frac{4k_{fg}(\Omega)\beta_2}{\gamma L}\frac{1}{\cos(\beta_1+\beta_2)} \tag{27}$$

Substituting Eq. (27) to Eq. (26) to eliminate the lateral force, we have the relationship of the deformation angles

$$\frac{\beta_1}{\beta_2} = \frac{k_{fg}(\Omega)}{k_b}\left[\left(\frac{1-\gamma}{\gamma}\right)\frac{\cos\beta_1}{\cos(\beta_1+\beta_2)}+1\right] \tag{28}$$

Given a specific lateral force F, we can always calculate the deformation angles β_1 and β_2 via any two equations from Eq. (26-28). Then one can find the lateral displacement x according to Eq. (25). With the lateral force and the solved lateral displacement, the lateral stiffness of the compliant parallelogram mechanisms with fixture compliance can be obtained

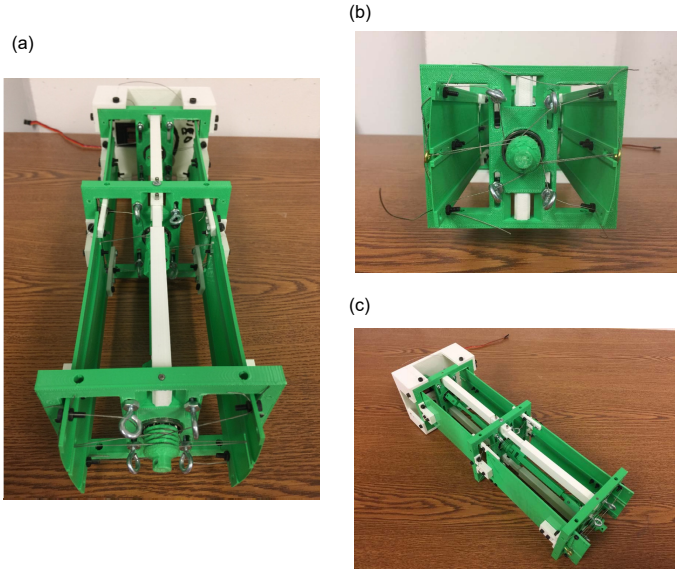

Morphing test

5 Experiment and testing

5.1 The 3D printed shape morphing arm

A robotic arm with tunable stiffness is fabricat printer with Acrylonitrile butadiene styrene (ABS) shown in Fig. 10. The detailed cable-driven mechanis in Fig. 10 (a) and (b), and the bearing frames and univ mission shafts are shown in Fig. 10 (c). The single m tuator is selected as HD 1235MG servo with a maxi of 3.954 Nm. The cable is selected as a coated st cable with a maximum force of 22.24 N. Eyebolts a the bending control pulleys and the base pulleys. N covering pulleys may not be required since the flexib provide a large recovery internal moment in the relea We wind the cables based on the routes described ir a single servo motor can continuously actuate the fle from the flattened shape to curved shapes, and vice maximum motor angle is 130° which corresponds t mum morphing angle of $\Omega = 90°$.

5.2 Lateral stiffness verification

We next test the variable lateral stiffness of the phing arm. The static testing setup is shown in Fig. 11. The shape morphing arm is clamped at the base to the table. A force sensor (M5-100, 500×0.1 N) bears against the end house of the compliant arm and can be driven to travel along the screw of the Mark-10 system (ES30, 1000 N). The displacement is measured by a travel display (ESM001, 150×0.01 mm). A laptop is used to collect the data from the sensors. The NI controller (controller (NI cRIO-9014) is used to continuously control the morphing angle of the compliant robotic arm.

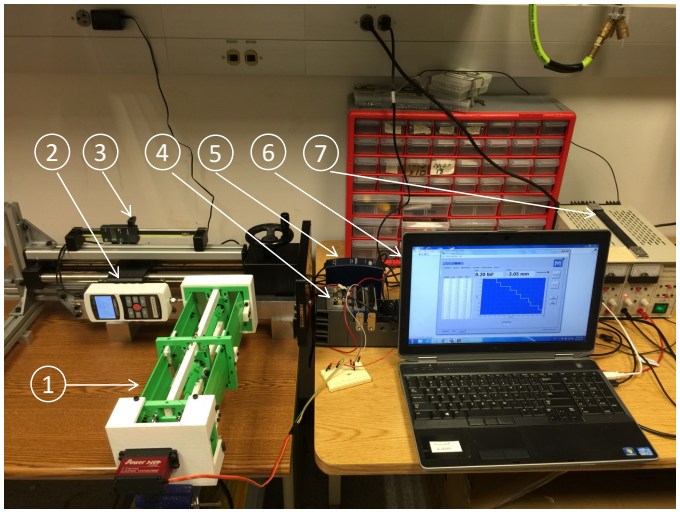

Figure 11 : The experiment setup for the static test. 1 The compliant robot arm, 2. The force sensor, 3. The travel display, 4 NI controller, 5 The power supply for NI controller, 6 Laptop collecting data, 7 The power supply for servo motor.

The servo motor is controlled from 0° to 130° with an increment of 10°. The lateral stiffness is calculated as the ratio of the lateral force over the lateral displacement. The experiment results of the lateral stiffness vs. the morphing angle are the "o" line as shown in Fig. 12. The theoretical estimation of the lateral stiffness with the original PRB model and the improved lateral stiffness model are shown the dashed line and solid line in Fig. 12, respectively. It is worth noting that E is set at 1.2 Gpa

and k_b is set at 20 N.m/rad according to the testing. We found that the improved PRB model can well predict the experiment results while the original PRB model deviates from the testing results. The experimental results show that a morphing angle from 0° to 90° can result in a lateral stiffness variation from 207 N/m to 458 N/m with a variety of 221.26%. In addition, the lateral stiffness with the PRB model also suggests that the lateral stiffness variation ratio of the shape morphing arm can be significantly improved if the boundary condition at the fixed end can be secured.

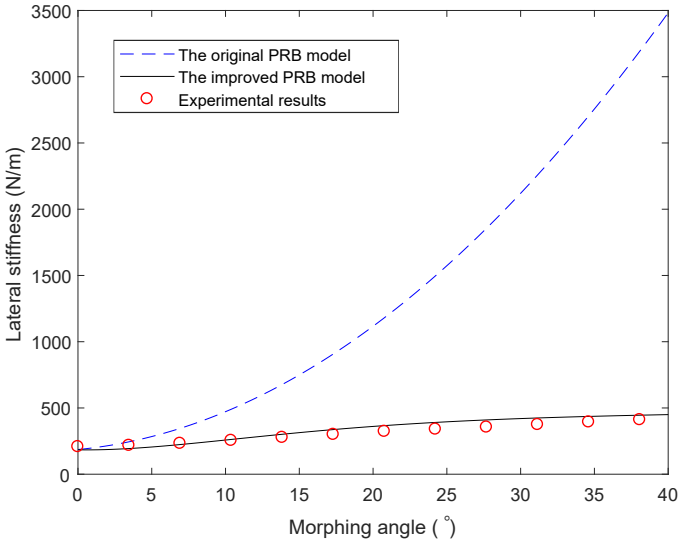

Figure 12 : Comparison of the original PRB model, the improved PRB model and experimental testing results for lateral stiffness.

6 Discussions

The modeling accuracy is significantly improved comparing the improved PRB model with the original PRB model for the lateral stiffness of the robotic arm. However, the improved PRB model does not perfectly estimate the experiment results. There may be a few reasons resulting in the modeling errors. For instance, the flexible beams may not be ideally uniformly morphed although three sets of the cable-driven mechanism are used. The non-uniformly shape morphing can result in the modeling errors. In addition, the transmission clearance and cable slackness may also introduce modeling errors. Last but not least, the 3D printed ABS beam introduces the anisotropy material property which may result in modeling errors as well.

In this study, the idea of morphing shape is simple but the realization of the actuation mechanisms is relatively complicated. The complex design is partially due to our goal of trying to minimize the number of actuators and to morph the beam shape uniformly and symmetrically as well as to increase the moment arm to reduce required motor torque. The proposed variable stiffness link design is by no means to replace other variable stiffness solutions such as the variable stiffness joints or actuators, but rather to provide an alternative solution or complementary solution to introduce mechanical compliance to the robotic system for safe physical human-robot interaction. Compared with other variable stiffness link designs in [27, 28, 29] which enable the robot link either rigid or compliant with switching mechanisms, this work developed an actively and continuously tunable stiffness arm with a relatively accurate lateral stiffness model.

A manipulator may be desired to have variable stiffness in any direction in space, which may require three orthogonal variable stiffnesses. In this study, the shape morphing arm is designed to allow the stiffness to be tunable only in its lateral direction while the stiffness in other directions is not tunable and barely affected. For a robotics system or mechanical system requiring tunable stiffness in an arbitrary direction, the appropriate assembling of three arms in series may be one of the solutions.

7 Conclusion

This paper presented a novel design of a tunable stiffness robot arm with cable-driven mechanisms for safe physical human-robot interaction. This study uses the the PRB model for kinematics analysis of the actuation mechanisms and lateral stiffness modeling of the shape morphing arm. It is found that the classical PRB model may not accurately predict the statics of the compliant parallelogram mechanism if the boundary condition is not perfectly rigid. We introduced additional torsional springs into modeling and the results show that the modeling accuracy is significantly improved. The testing results indicate that the lateral stiffness of the robot arm can achieve a variety of 221.26 % given a morphing angle of 90°. The experiment demonstrated the feasibility of introducing mechanical compliance into robot links and the possibility of applying the variable stiffness link for safe physical human-robot interactions.

Acknowledgment

This material is based upon work supported by the National Science Foundation under Grant No: CMMI-1637656. Any opinions, findings, and conclusions or recommendations expressed in this material are those of the author(s) and do not necessarily reflect the views of the funding agencies.

REFERENCES

[1] Mutlu, B., and Forlizzi, J., 2008. "Robots in organizations: the role of workflow, social, and environmental factors in human-robot interaction". In Human-Robot Interac-

tion (HRI), 2008 3rd ACM/IEEE International Conference on, IEEE, pp. 287–294.

[2] Wolf, S., and Hirzinger, G. "A new variable stiffness design: Matching requirements of the next robot generation". In IEEE International Conference on Robotics and Automation, 2008. ICRA 2008, pp. 1741–1746.

[3] Wolf, S., Eiberger, O., and Hirzinger, G. "The DLR FSJ: Energy based design of a variable stiffness joint". In 2011 IEEE International Conference on Robotics and Automation (ICRA), pp. 5082–5089.

[4] Friedl, W., Höppner, H., Petit, F., and Hirzinger, G. "Wrist and forearm rotation of the DLR hand arm system: Mechanical design, shape analysis and experimental validation". In 2011 IEEE/RSJ International Conference on Intelligent Robots and Systems, pp. 1836–1842.

[5] Ménard, T., Grioli, G., and Bicchi, A. "A stiffness estimator for agonistic #x2013;antagonistic variable-stiffness-actuator devices". *IEEE Transactions on Robotics,* **30**(5), pp. 1269–1278.

[6] Garabini, M., Passaglia, A., Belo, F., Salaris, P., and Bicchi, A. "Optimality principles in variable stiffness control: The VSA hammer". In 2011 IEEE/RSJ International Conference on Intelligent Robots and Systems, pp. 3770–3775.

[7] Schiavi, R., Grioli, G., Sen, S., and Bicchi, A. "VSA-II: a novel prototype of variable stiffness actuator for safe and performing robots interacting with humans". In IEEE International Conference on Robotics and Automation, 2008. ICRA 2008, pp. 2171–2176.

[8] Tonietti, G., Schiavi, R., and Bicchi, A. "Design and control of a variable stiffness actuator for safe and fast physical human/robot interaction". In Proceedings of the 2005 IEEE International Conference on Robotics and Automation, pp. 526–531.

[9] Zinn, M., Khatib, O., Roth, B., and Salisbury, J. K. "Playing it safe [human-friendly robots]". *IEEE Robotics Automation Magazine,* **11**(2), pp. 12–21.

[10] Migliore, S. A., Brown, E. A., and DeWeerth, S. P. "Biologically inspired joint stiffness control". In Proceedings of the 2005 IEEE International Conference on Robotics and Automation, pp. 4508–4513.

[11] Koganezawa, K. "Mechanical stiffness control for antagonistically driven joints". In 2005 IEEE/RSJ International Conference on Intelligent Robots and Systems, pp. 1544–1551.

[12] Pratt, G. A., and Williamson, M. M. "Series elastic actuators". In 1995 IEEE/RSJ International Conference on Intelligent Robots and Systems 95. 'Human Robot Interaction and Cooperative Robots', Proceedings, Vol. 1, pp. 399–406 vol.1.

[13] She, Y., Meng, D., Cui, J., and Su, H.-J., 2017. "On the impact force of human-robot interaction: Joint compliance vs. link compliance". In 2017 IEEE International Conference on Robotics and Automation (ICRA), IEEE, pp. 6718–6723.

[14] She, Y., Song, S., Su, H.-J., and Wang, J., 2020. "A comparative study on the effect of mechanical compliance for a safe physical human–robot interaction". *Journal of Mechanical Design,* **142**(6).

[15] Park, J.-J., Kim, B.-S., Song, J.-B., and Kim, H.-S. "Safe link mechanism based on nonlinear stiffness for collision safety". *Mechanism and Machine Theory,* **43**(10), pp. 1332–1348.

[16] Zhang, M., Laliberté, T., and Gosselin, C. "Force capabilities of two-degree-of-freedom serial robots equipped with passive isotropic force limiters". *Journal of Mechanisms and Robotics,* **8**(5), p. 051002.

[17] López-Martínez, J., Blanco-Claraco, J. L., García-Vallejo, D., and Giménez-Fernández, A. "Design and analysis of a flexible linkage for robot safe operation in collaborative scenarios". *Mechanism and Machine Theory,* **92**, pp. 1–16.

[18] She, Y., Su, H.-J., and Hurd, C. J., 2015. "Shape optimization of 2d compliant links for design of inherently safe robots". In ASME 2015 International Design Engineering Technical Conferences and Computers and Information in Engineering Conference, American Society of Mechanical Engineers, pp. V05BT08A004–V05BT08A004.

[19] She, Y., Su, H.-J., Meng, D., Song, S., and Wang, J., 2018. "Design and modeling of a compliant link for inherently safe corobots". *Journal of Mechanisms and Robotics,* **10**(1), p. 011001.

[20] Hines, L., Arabagi, V., and Sitti, M., 2012. "Shape memory polymer-based flexure stiffness control in a miniature flapping-wing robot". *IEEE Transactions on Robotics,* **28**(4), pp. 987–990.

[21] Galloway, K. C., Clark, J. E., and Koditschek, D. E., 2013. "Variable stiffness legs for robust, efficient, and stable dynamic running". *Journal of Mechanisms and Robotics,* **5**(1), p. 011009.

[22] She, Y., Su, H.-J., Lai, C., and Meng, D., 2016. "Design and prototype of a tunable stiffness arm for safe human-robot interaction". In ASME 2016 International Design Engineering Technical Conferences and Computers and Information in Engineering Conference, American Society of Mechanical Engineers Digital Collection.

[23] She, Y., Su, H.-J., Meng, D., and Lai, C., 2020. "Design and modeling of a continuously tunable stiffness arm for safe physical human–robot interaction". *Journal of Mechanisms and Robotics,* **12**(1).

[24] Howell, L. L., and Midha, A., 1994. "A method for the design of compliant mechanisms with small-length flexural pivots". *Journal of mechanical design,* **116**(1), pp. 280–290.

[25] Howell, L. L., and Midha, A., 1995. "Parametric deflection approximations for end-loaded, large-deflection beams in

compliant mechanisms". *Journal of Mechanical Design,* **117**(1), pp. 156–165.

[26] Howell, L. L., 2001. *Compliant mechanisms*. John Wiley & Sons.

[27] Park, J.-J., Kim, B.-S., Song, J.-B., and Kim, H.-S., 2008. "Safe link mechanism based on nonlinear stiffness for collision safety". *Mechanism and Machine Theory,* **43**(10), pp. 1332–1348.

[28] López-Martínez, J., Blanco-Claraco, J. L., García-Vallejo, D., and Giménez-Fernández, A., 2015. "Design and analysis of a flexible linkage for robot safe operation in collaborative scenarios". *Mechanism and Machine Theory,* **92**, pp. 1–16.

[29] Zhang, M., Laliberté, T., and Gosselin, C., 2016. "Force capabilities of two-degree-of-freedom serial robots equipped with passive isotropic force limiters". *Journal of Mechanisms and Robotics,* **8**(5), p. 051002.